(ANPA Conference 2024)
ISSN: 2392-473X(Print), 2738-9537 (Online)

Research Article ©Nepal Physical Society
DOI: https://doi.org/10.3126/jnphyssoc.v10i1.72828

Structural stability and electronic structure of (Ti, Ta)$_2$C MXenes

Saniya L. Lyles,[1, a)] Sadhana Vattikuti,[2, a)] Gabriel Kinney,[1, 3] Andrew Smith,[1, 3] Bhoj R. Gautam,[1] and Chandra M. Adhikari[1, b)]

[1)] *Department of Chemistry, Physics and Materials Science, Fayetteville State University, Fayetteville, NC 28301, USA*
[2)] *Panther Creek High School, Cary, NC 27519, USA*
[3)] *Cumberland International Early College High School, Fayetteville, NC 28301, USA*

[a)] *These authors contributed equally.*
[b)] *Corresponding author:cadhikari@uncfsu.edu*

Abstract. Graphene-like two-dimensional early transition metal carbides, nitrides, or carbonitrides with a metal-to-nonmetal atomic ratio of $(n+1)/n$ called MXenes have many excellent electronic, optical, and electrochemical properties, such as metallicity, high electrical conductivity, larger charge density, high capacitance, efficient lithium, sodium, and potassium ions intercalability, etc. First-principles Density Functional Theory (DFT) calculations are performed to study the structural relationship of (Ti, Ta)$_2$C MXenes to their electronic structure, magnetism, and optical properties. Calculations show carbide MXenes with a single transition metal, namely, titanium carbide (Ti$_2$C) and tantalum carbide (Ta$_2$C), and an ordered carbide MXene with double transition metals, namely, titanium tantalum carbide (TiTaC) are non-magnetic and metallic. The density of states at the Fermi level for each of (Ti, Ta)$_2$C MXenes is dominated by the outermost d-orbitals of transition metal and the $2p$ orbital of carbon. The dielectric response function is a photon energy-dependent anisotropic quantity. In the static limit, the imaginary parts of the dielectric functions vanish for each of the (Ti, Ta)$_2$C MXenes. However, the real part of the static dielectric constant is as high as two orders of magnitude for tantalum-containing MXenes and almost half of that for titanium-containing single transition metal carbide MXene.

Received: 25 August, 2024; **Revised**: October 18, 2024; **Accepted**: October 22, 2024

Keywords: MXenes; Double Transition Metal MXenes; Density Functional Theory, Titanium Carbides, Tantalam Carbides

1. INTRODUCTION

MXenes are graphene-like early transition metal carbides, nitrides, or carbonitrides with a stoichiometric formula of $M_{n+1}X_n$, where M is an early transition metal such as titanium(Ti), chromium(Cr), tantalum(Ta), etc., X is carbon(C) or nitrogen(N) or CN, and n is an integer greater than or equal to 1. Although some other processes of synthesizing pristine MXenes, such as direct synthesis and chemical vapor deposition (CVD), are also reported [1], a top-down selective etching of A-elements such as aluminum (Al) from MAX phases such as Ti_2AlC, TiTaAlC, Ta_2AlC, is the most common approach of MXene synthesis, which results in MXenes with tunable surface terminations such as -F, -O, -OH, and -H. Recently, MXenes have garnered significant attention due to their wide range of applications in energy storage, such as Li-ion batteries, and supercapacitors [2], electrocatalysts for hydrogen evolution reactions and oxygen evolution reactions [3], water purifiers [4], gas sensors [5], electrides as electron emitters [6, 7], and so on.

In 2015, Anasori et al. studied ordered double transition metal (DTM) carbides $M'_2M''C_2$ and $M'_2M'_2''C_3$ MXenes and predicted about two dozens of stable double transition metal carbides MXenes [8]. Having a unique combination of two early transition metals in their structures, DTM MXenes provide enhanced electronic, electrochemical, and optical features with diverse chemical functionalities compared to the single transition metal (STM) MXenes. Preparing $Ti_xTa_{4-x}C_3$ DTM MXenes via etching of Al atoms from their parent $Ti_xTa_{4-x}AlC_3$ MAX phases, Syamsai et al. [9] experimentally studied structural and electrochemical properties of $Ti_xTa_{4-x}C_3$ DTM MXenes and revealed that the DTM MXenes have a significant reversible high specific discharge capacity and capacity retention of about 97%. BY varying

the combination of transition metals, one can finely tune the properties of DTM MXenes. Some ordered DTM-MXenes with M′:M″::1:1 ratio shows better chemical stability compared to their single-metal counterparts such as $Ti_2Ta_2C_3$ MXene is found to be the most stable one out of the five stable $Ti_xTa_{4-x}C_3$ MXenes, where $x = 1,2,3,4$ [10]. Therein, the authors found that the ordered DTM $Ti_2Ta_2C_3$ has the lowest energy barrier among 5 of the $Ti_xTa_{4-x}C_3$ MXenes, and it can store four times more lithium than the pristine Ti_4C_3 MXene. These properties make the ordered DTM $Ti_2Ta_2C_3$ a preferred one among 5 of the $Ti_xTa_{4-x}C_3$ MXenes to be used as an anode in Li-ion batteries and energy storage applications.

STM Ti_2C and Ta_2C MXenes are widely studied theoretically and experimentally, investigating their electronic structure, magnetism, optical properties, electromechanical actuation, candidates for sodium and lithium-ion batteries anode, hydrogen storage medium, and so on [11-17]. This research presents a systematic study on ordered DTM TiTaC and compares it with associated STM Ti_2C and Ta_2C MXenes.

Carbon is a group *IVA* non metal with an electronic configuration of $1s^2,\ 2s^2\,2p^2$. The $3d$ transition metal Ti has an electronic configuration of $1s^2,\ 2s^2\,2p^6,\ 3s^2\,3p^6,\ 3d^2\,4s^2$ and that for the $5d$ transition metal Ta is $1s^2,\ 2s^2\,2p^6,\ 3s^2\,3p^6,\ 3d^{10}\,4s^2\,4p^6,\ 4d^{10}\,4f^{14}\,5s^2\,5p^6,\ 5d^4\,6s^1$. How C interacts with $3d$ transition metal versus $5d$ transition metal and its behavior in the presence of both $3d$ and $5d$ transition metals at the quantum mechanical level is of great interest. For our chosen pseudopotentials, we have valence electrons in $2s^2\,2p^2$ for C, $3p^6,\ \ 3d^2\,4s^2$ for Ti, and $5p^6,\ 5d^4\,6s^1$ for Ta.

2. STRUCTURAL ANALYSIS

A top-down method of immersing Ti_2AlC MAX phase powder with hydrofluoric acid (HF) or a mixture of lithium fluoride (LiF) with hydrochloric acid (HCl) and removing Al-layers from the MAX phase results in a Ti_2C MXene with rhombohedral lattice and trigonal crystal system, which lies in the $R\bar{3}m$ space group (#166). In a Ti_2C unit cell, Ti atoms reside in $6c$ Wyckoff position with atomic coordinates of (0,0, 0.245498) while C atoms are at $3b$ Wyckoff position with the coordinates of (1/3, 2/3, 1/6). Each Ti in Ti_2C is bonded to three equivalent C atoms in a triangular non-coplanar chemical environment, whereas each C atom is bonded to six equivalent Ti atoms to form edge-sharing CTi_6 octahedra. Ta_2C MXene prefers to have a trigonal crystal structure in a hexagonal lattice system with a space group of $P\bar{3}m1$ (#164). Ta atom occupies the $2d$ Wyckoff position with atomic coordinates of (1/3, 2/3, 0.253899) in a triangular non-coplanar environment, whereas the C atom resides in the $1a$ Wyckoff position at the origin. Ta in Ta_2C is

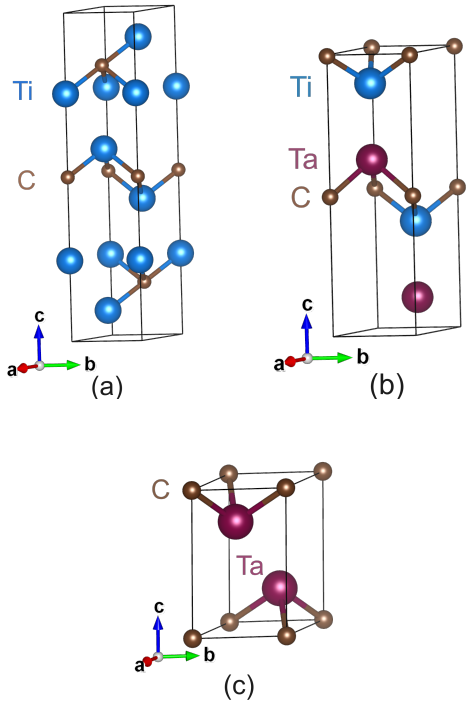

FIGURE 1: Unit cells of computationally optimized Ti_2C (a), TiTaC (b), and Ta_2C (c) MXenes showing side view along the rotated a-axis.

caged in distorted octahedra maintaining 3-fold rotational symmetry, while the C-centered polyhedron forms a trigonal prism surrounded by Ta and symmetric with respect to 120° rotation. TiTaC crystalizes to a hexagonal structure with a primitive lattice type whose space group and number are $P6_3mc$ and 186. Ti is at a $2b$ Wyckoff site with the atomic coordinates of (1/3, 2/3, 0.38765), Ta is at a $2b$ Wyckoff site with the atomic coordinates of (1/3, 2/3, 0.11672), and C is at Wyckoff $2a$ position with atomic coordinates of (0.00000, 0.00000, -0.00437). The unit cell of Ti_2C, TiTaC, and Ta_2C contains 9, 6, and 3 atoms, respectively. The structure parameters for optimized Ti_2C, TiTaC, and Ta_2C are presented in Table I. For Ti_2C and Ta_2C, the unit cell's computed lattice parameters, angles, and volume are in good agreement with experimental measurement. The c/a ratio is about 1.6 in Ta_2C, while this is about 4.7 in Ti_2C and 3.4 in TiTaC. Figure 1 shows unit cells of computationally optimized crystal structures of Ti_2C, TiTaC, and Ta_2C MXenes. To understand the magnetic properties of the MXenes under consideration, we compared each crystal's structural and formation energy with all possible magnetic phases. The calculations confirm that all the Ti_2C, TiTaC, and Ta_2C MXenes favor the nonmagnetic phases.

Initial crystal structures are adopted from a core program of the Materials Genome Initiative using high-throughput computing to uncover the properties of in-

TABLE I: Structure parameters for computationally optimized structures of (Ti, Ta)$_2$C MXenes. Experimentally measured values for chosen structures of Ti_2C [18] and Ta_2C at 293K [19] are given in parenthesis. As the chosen crystal systems here for theoretical study are the same as experimental references, the angles are in perfect agreement. To the best of our knowledge, no data are available for TiTaC.

MXenes	a (Å)	b(Å)	c (Å)	α (degree)	β (degree)	γ (degree)	Unit cell volume (Å^3)
Ti_2C	3.075 (3.062)	3.075 (3.062)	14.421 (14.910)	90.000	90.000	120.000	118.070
TiTaC	3.056	3.056	10.508	90.000	90.000	120.000	84.993
Ta_2C	3.115 (3.106)	3.115 (3.106)	4.939 (4.946)	90.000	90.000	120.000	41.503 (41.3)

organic materials called Materials Project [20]. The Visualisation for Electronic STructural Analysis (VESTA) program was used for the crystallographic presentations.

3. COMPUTATIONAL METHODS

The first-principles Density Functional Theory (DFT) calculations [21] were performed with the Vienna Ab initio Simulation Package (VASP) [22-24], which is written primarily in Fortran and uses either effective Vanderbilt potentials or the projector augmented wave (PAW) method [25], and a plane wave basis set. The Perdew-Burke-Ernzerhof (PBE) parametrization of the generalized gradient approximation (GGA) described the electron-electron exchange and correlation functions [26]. The plane wave cutoff energy of 520 eV was used. The electronic iterations convergence criteria of 10^{-5} eV for energy and 10^{-2} eV/Å for force using the Normal (blocked Davidson) algorithm and reciprocal space projection operators are used. The Gaussian smearing with a width of 0.05 eV was used to speed up the convergence. The k-mesh of $12\times12\times3$ was used for structure optimization and $17\times17\times5$ mesh for the density of states and optical spectra calculations for Ti_2C and TiTaC, while the same for Ta_2C are $12\times12\times12$ and $17\times17\times17$. The k-mesh is forced to be centered on the gamma point and have an odd number of points in each direction.

4. RESULTS AND DISCUSSION

The formation energy $E_f(\mathrm{Ti}_x\mathrm{Ta}_{2-x}\mathrm{C})$ of (Ti, Ta)$_2$C MXenes in its bulk phase reads

$$E_f(\mathrm{Ti}_x\mathrm{Ta}_{2-x}\mathrm{C}) = \frac{1}{3}\Big[E(\mathrm{Ti}_x\mathrm{Ta}_{2-x}\mathrm{C}) - xE(\mathrm{Ti}) - (2-x)E(\mathrm{Ta}) - E(\mathrm{C})\Big], \quad (1)$$

where x is 2 for Ti_2C, 1 for TiTaC and 0 for Ta_2C. The calculated formation energies of the $E_f(Ti_2C)$, $E_f(Ta_2C)$ and E_f(TiTaC) are respectively, -0.682, -0.438 and -0.575 eV/atom indicating that $E_f(Ti_2C)$ is the most stable one among them considering only the formation energy into account. The negative formation energy value of E_f(TiTaC) indicates the stability of the ordered DTM carbide TiTaC MXene along with its STM carbides MXenes.

Band structures and density of states of Ti_2C, TiTaC, and Ta_2C MXenes are shown in Figs. 2, 3, and 4. All of the MXenes under consideration in this article have no band gap and are, hence, metallic in nature. The DOS of Ti_2C is dominated by $3d$ states of Ti in the Fermi level and the conduction band, while the $2p$ states of C and $3d$ states of Ti hybridize in the valence band. The hybridization is strong, and Ti$-3d$ states and C$-2p$ have almost overlapped peaks at energy around -2.7 eV measured from the Fermi level indicating a Ti-C covalent band. In TiTaC, the projected DOS of Ti$-3d$ and Ta$-5d$ hybridize almost for all energy values. In Ta_2C, the DOS is dominated by Ta$-5d$ states while we witness the significant contributions from the $2p$ states of C and $5p$ states of Ta.

Optical responses of any material interacting with light can be exploited from its dielectric function (ε). The complex dielectric functions of Ti_2C, TiTaC, and Ta_2C MXenes are calculated as a function of energy, divided each of these functions by the value of the absolute dielectric constant value of free space to obtain permittivities relative to air, and presented in Fig. 5. For better comparison, permittivities relative to air are plotted in the same photon energy ranges. The complex dielectric function of each MXenes under consideration here is isotropic within the $x-y$ plane while anisotropic along the $x-y$ plane versus an axis perpendicular to the plane. At zero energy, i.e., $\omega = 0$, the imaginary part of ε is zero for each of them, indicating no light absorption, while the materials behave dielectric with permittivity as high as 145 along the x-axis for TiTaC. The real parts of εs at zero energy are the least for Ti_2C among the three MXenes. The Reε_x to Reε_z ratio at zero energy is more than 2 in TiTaC DTM, while the ratio is almost unity for Ti_2C and Ta_2C STMs. Note that the $\omega = 0$ case gives the static value of the dielectric response. In the visible range, i.e., 1.63 to 3.26 eV, the real part of εs is smaller than in the low energy region for all three MXenes, while the imaginary parts in the same region are not constant but remain almost 20

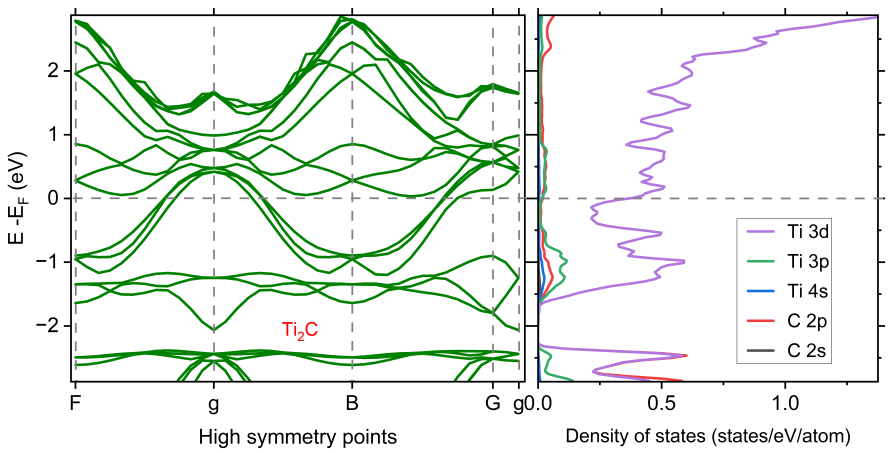

FIGURE 2: Band structure (left panel) and orbital resolved density of states (right panel) of Ti_2C MXene. Energy values are shifted by Fermi energy (E_F) such that the Fermi level will be at zero level.

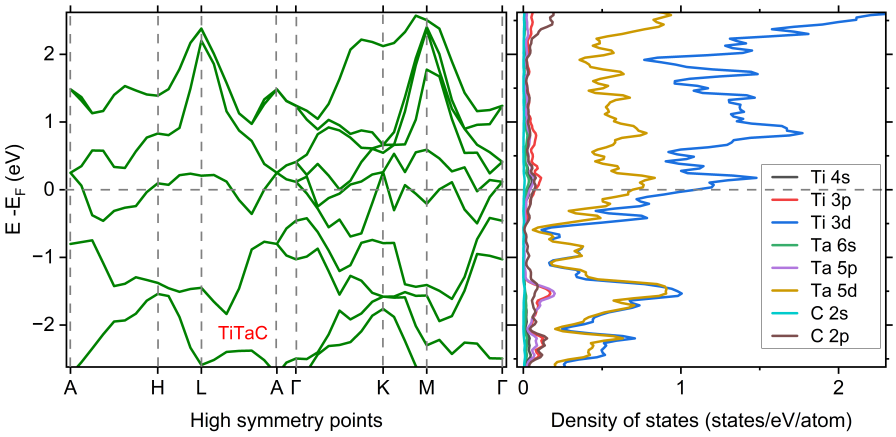

FIGURE 3: Band structure (left panel) and orbital resolved density of states (right panel) of TiTaC MXene. Energy values are shifted by E_F such that the Fermi level will be at zero level.

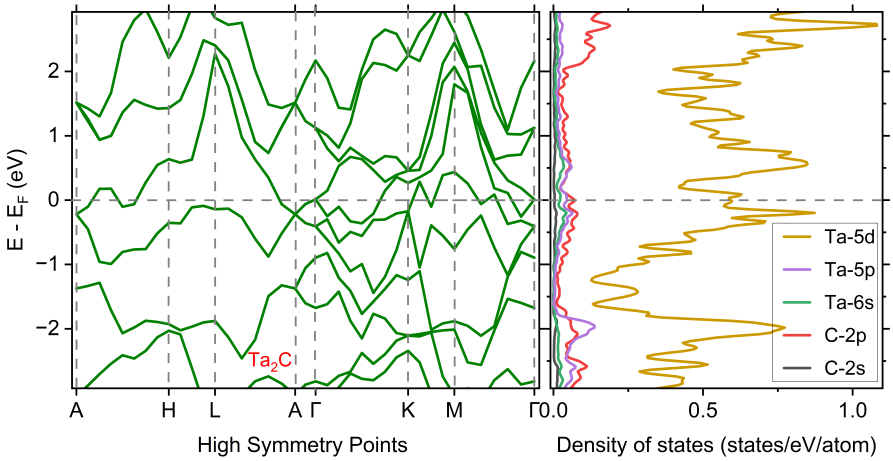

FIGURE 4: Band structure (left panel) and orbital resolved density of states (right panel) of Ta_2C MXene. Energy values are shifted by E_F such that the Fermi level will be at zero level.

along both in-plane and out-of-plane directions. In the ultraviolet range, i.e., beyond 3.26 eV, the real part of ε

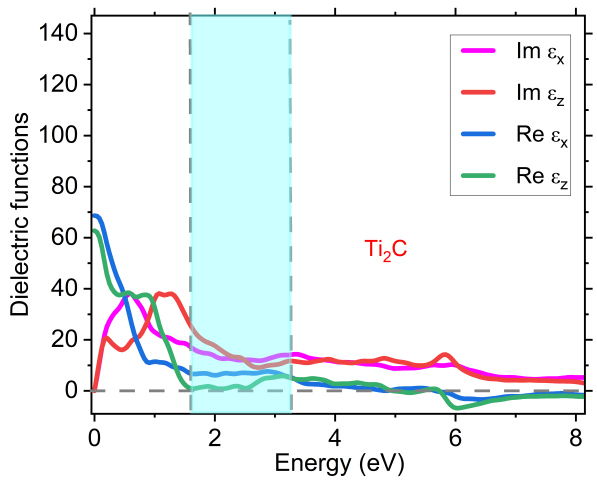

(a)

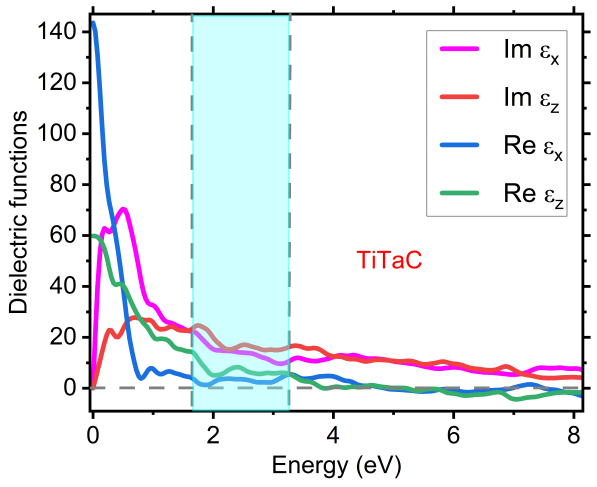

(b)

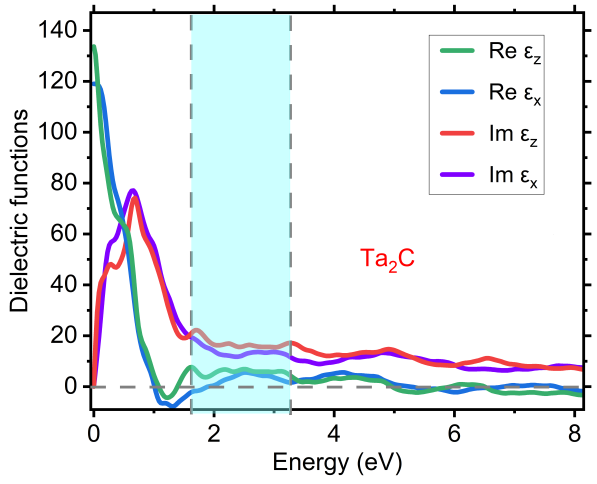

(c)

FIGURE 5: Dielectric functions of Ti_2C, TiTaC, and Ta_2C MXenes as a function of energy. The sky-blue shaded region shows the visible range of the electromagnetic spectrum.

remains around zero values, and the imaginary parts have an order of magnitude. In the infrared range, i.e., 1.24 to 1.63 eV, the imaginary part of $\varepsilon(\omega)$ for Ta_2C is negative, indicating natural passivity of Ta_2C near the Fabry-Perot resonances [27, 28].

A brief discussion on how the dielectric function relates to other physical quantities, such as conductivity and refractive index, is in order. One can write the complex frequency (energy)-dependent dielectric function as

$$\varepsilon(\omega) = \varepsilon_1(\omega) + \mathrm{i}\,\varepsilon_2(\omega), \tag{2}$$

where $\varepsilon_1(\omega)$ and $\varepsilon_2(\omega)$ are the real and imaginary part of the $\varepsilon(\omega)$. Then the complex conductivity reads

$$\sigma(\omega) = \sigma_1(\omega) + \mathrm{i}\,\sigma_2(\omega), \tag{3}$$

where the real $\sigma_1(\omega)$ and imaginary $\sigma_2(\omega)$ parts of the conductivity are given by

$$\sigma_1(\omega) = \frac{\omega}{4\pi}\varepsilon_2(\omega), \tag{4}$$

and

$$\sigma_2(\omega) = \frac{\omega}{4\pi}\left[\varepsilon_\infty - \varepsilon_1(\omega)\right]. \tag{5}$$

Here, ε_∞ represents the high-frequency dielectric constant and usually unity for frequencies where the free carriers are responsible for the material's response.

Keeping in mind that the dielectric function is a complex quantity, we can express the relation between the refractive index $\eta(\omega)$ and the dielectric function $\varepsilon(\omega)$ as

$$\eta(\omega) + \mathrm{i}\,\mathrm{k}(\omega) = \sqrt{\varepsilon_1(\omega) + \mathrm{i}\varepsilon_2(\omega)} \tag{6}$$

where $k(\omega)$ is an extinction coefficient, which measures the amount of light absorbed by a material when light propagates through it. One can solve for $\eta(\omega)$ and $k(\omega)$ to get

$$\eta(\omega) = \sqrt{\frac{\varepsilon_1(\omega) + \sqrt{\varepsilon_1^2(\omega) + \varepsilon_2^2(\omega)}}{2}}. \tag{7}$$

and

$$k(\omega) = \sqrt{\frac{-\varepsilon_1(\omega) + \sqrt{\varepsilon_1^2(\omega) + \varepsilon_2^2(\omega)}}{2}}. \tag{8}$$

The larger values of real, imaginary, or both result in a larger value of the refractive index. However, the extinction coefficient depends on some complicated mathematical relation being primarily dependent on the imaginary part of the $\varepsilon(\omega)$.

5. CONCLUSION

The electronic structures and optics of two STMs, Ti_2C and Ta_2C, and a TiTaC DTM, have been analyzed using the first-principles quantum mechanical DFT calculation using VASP. Comparing the formation energy values, Ti_2C is the most stable among the three MXenes of interest in the article. All three (Ti, Ta)$_2$C are metallic and nonmagnetic in their pristine phases. In Ti_2C, the DOS is dominated by Ti$-3d$ states in the conduction band and the Fermi level, while Ti$-3d$ and C$-2p$ states dominate the valence band. Strong hybridization of Ti$-3d$ and C$-2p$ states in the valence band and peaks at the energy around -2.7 eV below Fermi level confirms the existence of Ti$-$C covalent bond in Ti_2C. In the TiTaC valence band, there is a domination and strong hybridization of Ti$-3d$ and Ta$-5d$ states while with some contributions from C$-2p$, Ta$-5p$ and Ti$-3p$ states. The conduction band of TiTaC is dominated by Ti$-3d$ and Ta$-5d$ states. In Ta_2C MXene, the DOS in the valence band is dominated by Ta$-5d$ with some contributions from Ta$-5p$ and C$-2p$ states. In the conduction band, the DOS of Ta_2C is dominated by Ta$-5d$ states.

The optical response of (Ti, Ta)$_2$C MXenes are photon's energy dependent. The static value of each imaginary part of each MXenes under consideration in this work is zero. The static value of dielectric response for Ta_2C for each in-plane and out-of-plane is almost double that of corresponding components of Ti_2C. An interesting thing happens when Ti and Ta are in a 1:1 atomic ratio in (Ti, Ta)$_2$C MXenes. Anisotropy in dielectric responses is enhanced heavily even at the $\omega = 0$ limit, resulting in Re ε_x /Re ε_z >2. In the visible range, the real parts of $\varepsilon(\omega)$ for all (Ti, Ta)$_2$C MXenes are about an order of magnitude.

ACKNOWLEDGMENTS

This work is supported by the Department of Energy BES-RENEW award number DE-SC0024611.

EDITORS' NOTE

This manuscript was submitted to the Association of Nepali Physicists in America (ANPA) Conference 2024 for publication in the special issue of the Journal of Nepal Physical Society.

REFERENCES

1. D. Wang, C. Zhou, A. S. Filatov, W. Cho, F. Lagunas, M. Wang, S. Vaikuntanathan, C. Liu, R. F. Klie, and D. V. Talapin, "Direct synthesis and chemical vapor deposition of 2D carbide and nitride MXenes," Science **379**, 1242–1247 (2023).
2. X. Li, Z. Huang, C. E. Shuck, and Y. Gogotsi, "MXene chemistry, electrochemistry and energy storage applications," Nature Reviews Chemistry **6**, 389–404 (2022).
3. M. Zubair, M. M. Ul Hassan, M. T. Mehran, M. M. Baig, S. Hussain, and F. Shahzad, "2D MXenes and their heterostructures for HER, OER and overall water splitting: A review," International Journal of Hydrogen Energy **47**, 2794–2818 (2022).
4. C. E. Ren, K. B. Hatzell, M. Alhabeb, Z. Ling, K. A. Mahmoud, and Y. Gogotsi, "Charge- and Size-Selective Ion Sieving Through $Ti_3C_2T_x$ MXene Membranes," The Journal of Physical Chemistry Letters **6**, 4026–4031 (2015).
5. S. J. Kim, H.-J. Koh, C. E. Ren, O. Kwon, K. Maleski, S.-Y. Cho, B. Anasori, C.-K. Kim, Y.-K. Choi, J. Kim, Y. Gogotsi, and H.-T. Jung, "Metallic $Ti_3C_2T_x$ MXene Gas Sensors with Ultrahigh Signal-to-Noise Ratio," ACS Nano **12**, 986–993 (2018).
6. C. M. Adhikari, D. Thapa, T. D. Alexander, C. K. Addaman, S. Han, B. P. Bastakoti, D. E. Autrey, S. Kilina, B. K. Rai, and B. R. Gautam, "Confinement of quasi-atomic structures in Ti_2N and Ti_3N_2 MXene Electrides," (2024), arXiv:2408.00897 [cond-mat.mtrl-sci].
7. L. M. McRae, R. C. Radomsky, J. T. Pawlik, D. L. Druffel, J. D. Sundberg, M. G. Lanetti, C. L. Donley, K. L. White, and S. C. Warren, "Sc_2C, a 2D Semiconducting Electride," Journal of the American Chemical Society **144**, 10862–10869 (2022).
8. B. Anasori, Y. Xie, M. Beidaghi, J. Lu, B. C. Hosler, L. Hultman, P. R. C. Kent, Y. Gogotsi, and M. W. Barsoum, "Two-Dimensional, Ordered, Double Transition Metals Carbides (MXenes)," ACS Nano **9**, 9507–9516 (2015).
9. R. Syamsai, J. R. Rodriguez, V. G. Pol, Q. V. Le, K. M. Batoo, S. F. Adil, S. Pandiaraj, M. R. Muthumareeswaran, E. H. Raslan, and A. N. Grace, "Double transition metal MXene ($Ti_xTa_{4-x}C_3$) 2D materials as anodes for Li-ion batteries," Scientific Reports **11**, 688 (2021).
10. D. Maldonado-Lopez, J. R. Rodriguez, V. G. Pol, R. Syamsai, N. G. Andrews, S. J. Gutiérrez-Ojeda, R. Ponce-Pérez, M. G. Moreno-Armenta, and J. Guerrero-Sánchez, "Atomic-Scale Understanding of Li Storage Processes in the Ti_4C_3 and Chemically Ordered $Ti_2Ta_2C_3$ MXenes: A Theoretical and Experimental Assessment," ACS Applied Energy Materials **5**, 1801–1809 (2022).
11. B. Wu, X. Cai, L. Shui, E. Gao, and Z. Liu, "Extraordinary Electromechanical Actuation of Ti_2C MXene," The Journal of Physical Chemistry C **125**, 1060–1068 (2021).
12. M. Kurtoglu, M. Naguib, Y. Gogotsi, and M. W. Barsoum, "First principles study of two-dimensional early transition metal carbides," MRS Communications **2**, 133–137 (2012).
13. M. Naguib, Y. Gogotsi, and M. W. Barsoum, "Mxenes: A New Family of Two-Dimensional Materials and Its Application As Electrodes for Li and Na-Ion Batteries," ECS Meeting Abstracts **MA2015-01**, 849 (2015).
14. Q. Hu, D. Sun, Q. Wu, H. Wang, L. Wang, B. Liu, A. Zhou, and J. He, "MXene: A New Family of Promising Hydrogen Storage Medium," The Journal of Physical Chemistry A **117**, 14253–14260 (2013).
15. M. Naguib, J. Come, B. Dyatkin, V. Presser, P.-L. Taberna, P. Simon, M. W. Barsoum, and Y. Gogotsi, "MXene: a promising transition metal carbide anode for lithium-ion batteries," Electrochemistry Communications **16**, 61–64 (2012).
16. I. Shein and A. Ivanovskii, "Graphene-like titanium carbides and nitrides $Ti_{n+1}C_n$, $Ti_{n+1}N_n$ (n=1, 2, and 3) from de-intercalated MAX phases: First-principles probing of their structural, electronic properties and relative stability," Computational Materials Science **65**, 104–114 (2012).
17. O. Udoh, A. Briles, B. Gautam, and D. E. Autrey, "Effect of Etching Method on the Morphology and Stability of Ti_2CT_x MXene," Microscopy and Microanalysis **28**, 2800–2801 (2022).

18. C. H. de Novion, B. Beuneu, T. Priem, N. Lorenzelli, and A. Finel, "The Physics and Chemistry of Carbides, Nitrides and Borides," in *NATO ASI Series E*, Vol. 185 (Springer, Dordrecht, 1990).
19. F. Lissner and T. Schleid, "Refinement of the crystal structure of ditantalum monocarbide, Ta_2C," Zeitschrift fur Kristallographie - New Crystal Structures **216**, 351–352 (2001).
20. A. Jain, S. P. Ong, G. Hautier, W. Chen, W. D. Richards, S. Dacek, S. Cholia, D. Gunter, D. Skinner, G. Ceder, and K. A. Persson, "Commentary: The Materials Project: A materials genome approach to accelerating materials innovation," APL Materials **1**, 011002 (2013).
21. W. Kohn and L. J. Sham, "Self-Consistent Equations Including Exchange and Correlation Effects," Phys. Rev. **140**, A1133–A1138 (1965).
22. G. Kresse and J. Hafner, "Ab initio molecular dynamics for liquid metals," Phys. Rev. B **47**, 558–561 (1993).
23. G. Kresse and J. Furthmüller, "Efficiency of ab-initio total energy calculations for metals and semiconductors using a plane-wave basis set," Computational Materials Science **6**, 15–50 (1996).
24. G. Kresse and J. Furthmüller, "Efficient iterative schemes for ab initio total-energy calculations using a plane-wave basis set," Phys. Rev. B **54**, 11169–11186 (1996).
25. P. E. Blöchl, "Projector augmented-wave method," Phys. Rev. B **50**, 17953–17979 (1994).
26. J. P. Perdew, K. Burke, and M. Ernzerhof, "Generalized Gradient Approximation Made Simple," Phys. Rev. Lett. **77**, 3865–3868 (1996).
27. K.-L. Zhang, Z.-L. Hou, L.-B. Kong, H.-M. Fang, and K.-T. Zhan, "Origin of Negative Imaginary Part of Effective Permittivity of Passive Materials," Chinese Physics Letters **34**, 097701 (2017).
28. C. M. Adhikari, D. Dahal, S. Kunwar, and B. R. Gautam, "Ti_3C_2 and Ti_2C MXenes based distributed Bragg reflectors in Fabry Perot cavity's resonance tuning," (2024), accepted for publication in Journal of Electronic Materials.